



**HAL**  
open science

## Ecosystem transpiration and evaporation: Insights from three water flux partitioning methods across FLUXNET sites

Jacob Nelson, Oscar Pérez-priego, Sha Zhou, Rafael Poyatos, Yao Zhang, Peter Blanken, Teresa Gimeno, Georg Wohlfahrt, Ankur Desai, Beniamino Gioli, et al.

### ► To cite this version:

Jacob Nelson, Oscar Pérez-priego, Sha Zhou, Rafael Poyatos, Yao Zhang, et al.. Ecosystem transpiration and evaporation: Insights from three water flux partitioning methods across FLUXNET sites. *Global Change Biology*, 2020, 26 (12), pp.6916-6930. 10.1111/gcb.15314 . hal-02995533

**HAL Id: hal-02995533**

**<https://hal.univ-lorraine.fr/hal-02995533>**

Submitted on 7 Jun 2022

**HAL** is a multi-disciplinary open access archive for the deposit and dissemination of scientific research documents, whether they are published or not. The documents may come from teaching and research institutions in France or abroad, or from public or private research centers.

L'archive ouverte pluridisciplinaire **HAL**, est destinée au dépôt et à la diffusion de documents scientifiques de niveau recherche, publiés ou non, émanant des établissements d'enseignement et de recherche français ou étrangers, des laboratoires publics ou privés.



Distributed under a Creative Commons Attribution 4.0 International License

# Ecosystem transpiration and evaporation: Insights from three water flux partitioning methods across FLUXNET sites

Jacob A. Nelson<sup>1</sup>  | Oscar Pérez-Priego<sup>2</sup> | Sha Zhou<sup>3,4,5</sup> | Rafael Poyatos<sup>6,7</sup>  | Yao Zhang<sup>3</sup>  | Peter D. Blanken<sup>8</sup> | Teresa E. Gimeno<sup>9,10</sup> | Georg Wohlfahrt<sup>11</sup> | Ankur R. Desai<sup>12</sup> | Beniamino Gioli<sup>13</sup>  | Jean-Marc Limousin<sup>14</sup> | Damien Bonal<sup>15</sup> | Eugénie Paul-Limoges<sup>16</sup> | Russell L. Scott<sup>17</sup> | Andrej Varlagin<sup>18</sup> | Kathrin Fuchs<sup>19</sup>  | Leonardo Montagnani<sup>20</sup>  | Sebastian Wolf<sup>21</sup> | Nicolas Delpierre<sup>22</sup>  | Daniel Berveiller<sup>22</sup> | Mana Gharun<sup>21</sup> | Luca Belelli Marchesini<sup>23,24</sup>  | Damiano Gianelle<sup>23</sup>  | Ladislav Šigut<sup>25</sup>  | Ivan Mammarella<sup>26</sup> | Lukas Siebicke<sup>27</sup> | T. Andrew Black<sup>28</sup> | Alexander Knohl<sup>27,29</sup> | Lukas Hörtnagl<sup>30</sup> | Vincenzo Magliulo<sup>31</sup> | Simon Besnard<sup>1,32</sup>  | Ulrich Weber<sup>1</sup> | Nuno Carvalhais<sup>1,33</sup> | Mirco Migliavacca<sup>1</sup> | Markus Reichstein<sup>1,34</sup> | Martin Jung<sup>1</sup>

<sup>1</sup>Department of Biogeochemical Integration, Max Planck Institute for Biogeochemistry, Jena, Germany

<sup>2</sup>Department of Biological Sciences, Macquarie University, Sydney, NSW, Australia

<sup>3</sup>Lamont-Doherty Earth Observatory of Columbia University, Palisades, NY, USA

<sup>4</sup>Earth Institute, Columbia University, New York, NY, USA

<sup>5</sup>Department of Earth and Environmental Engineering, Columbia University, New York, NY, USA

<sup>6</sup>CREAF, Cerdanyola del Vallès, Spain

<sup>7</sup>Universitat Autònoma de Barcelona, Cerdanyola del Vallès, Spain

<sup>8</sup>Department of Geography, University of Colorado, Boulder, CO, USA

<sup>9</sup>Basque Centre for Climate Change, Scientific Campus of the University of the Basque Country, Leioa, Spain

<sup>10</sup>IKERBASQUE, Basque Foundation for Science, Bilbao, Spain

<sup>11</sup>Department of Ecology, University of Innsbruck, Innsbruck, Austria

<sup>12</sup>Department of Atmospheric and Oceanic Sciences, University of Wisconsin-Madison, Madison, WI, USA

<sup>13</sup>Institute of Bioeconomy (IBE), National Research Council of Italy (CNR), Firenze, Italy

<sup>14</sup>CEFE, UMR 5175, CNRS, Univ Montpellier, Univ Paul Valéry Montpellier 3, EPHE, IRD, Montpellier, France

<sup>15</sup>Université de Lorraine, AgroParisTech, INRA, UMR Silva, Nancy, France

<sup>16</sup>Department of Geography, University of Zurich, Zurich, Switzerland

<sup>17</sup>Southwest Watershed Research Center, USDA-ARS, Tucson, AZ, USA

<sup>18</sup>A.N. Severtsov Institute of Ecology and Evolution, Russian Academy of Sciences, Moscow, Russia

<sup>19</sup>Karlsruhe Institute of Technology (KIT) Institute of Meteorology and Climate Research – Atmospheric Environmental Research, Garmisch-Partenkirchen, Germany

<sup>20</sup>Forest Service, Autonomous Province of Bolzano-Bozen, Bolzano-Bozen, Italy

<sup>21</sup>Department of Environmental Systems Science, ETH Zurich, Zurich, Switzerland

<sup>22</sup>Ecologie Systématique Evolution, Univ. Paris-Sud, CNRS, AgroParisTech, Université Paris-Saclay, Orsay, France

<sup>23</sup>Department of Sustainable Agro-Ecosystems and Bioresources, Research and Innovation Centre, Fondazione Edmund Mach, San Michele all'Adige, Italy

<sup>24</sup>Department of Landscape Design and Sustainable Ecosystems, Agrarian-Technological Institute, RUDN University, Moscow, Russia

<sup>25</sup>Department of Matter and Energy Fluxes, Global Change Research Institute of the Czech Academy of Sciences, Brno, Czech Republic

-----  
This is an open access article under the terms of the Creative Commons Attribution License, which permits use, distribution and reproduction in any medium, provided the original work is properly cited.

© 2020 The Authors. *Global Change Biology* published by John Wiley & Sons Ltd

<sup>26</sup>Institute for Atmospheric and Earth System Research INAR/Physics, Faculty of Science, University of Helsinki, Helsinki, Finland

<sup>27</sup>Bioclimatology, University of Goettingen, Göttingen, Germany

<sup>28</sup>Faculty of Land and Food Systems, University of British Columbia, Vancouver, BC, Canada

<sup>29</sup>Centre of Biodiversity and Sustainable Land Use, University of Goettingen, Goettingen, Germany

<sup>30</sup>Institute of Agricultural Sciences, ETH Zurich, Zurich, Switzerland

<sup>31</sup>Institute for Agricultural and Forest Systems in the Mediterranean (ISAFoM), National Research Council of Italy (CNR), Ercolano, Italy

<sup>32</sup>Laboratory of Geo-Information Science and Remote Sensing, Wageningen University and Research Center, Wageningen, The Netherlands

<sup>33</sup>Faculdade de Ciências e Tecnologia, FCT, Universidade Nova de Lisboa, Lisbon, Portugal

<sup>34</sup>Michael-Stifel-Center Jena for Data-Driven and Simulation Science, Jena, Germany

#### Correspondence

Jacob A. Nelson, Department of Biogeochemical Integration, Max Planck Institute for Biogeochemistry, Jena, Germany.  
Email: jnelson@bgc-jena.mpg.de

#### Funding information

Swiss National Science Foundation, Grant/Award Number: 20FI20\_173691; Ministry of Education, Youth and Sports of the Czech Republic, Grant/Award Number: LM2015061; SustES-Adaptation strategies, Grant/Award Number: CZ.02.1.01/0.0/0.0/16\_019/0000797; Austrian National Science, Grant/Award Number: I03859; Province of South Tyrol; Humboldt Research Fellowship for Experienced Researchers, Grant/Award Number: CGL2014-55883-JIN and RTI2018-095297-J-I00; Open access funding enabled and organized by Projekt DEAL.

#### Abstract

We apply and compare three widely applicable methods for estimating ecosystem transpiration ( $T$ ) from eddy covariance (EC) data across 251 FLUXNET sites globally. All three methods are based on the coupled water and carbon relationship, but they differ in assumptions and parameterizations. Intercomparison of the three daily  $T$  estimates shows high correlation among methods ( $R$  between .89 and .94), but a spread in magnitudes of  $T/ET$  (evapotranspiration) from 45% to 77%. When compared at six sites with concurrent EC and sap flow measurements, all three EC-based  $T$  estimates show higher correlation to sap flow-based  $T$  than EC-based  $ET$ . The partitioning methods show expected tendencies of  $T/ET$  increasing with dryness (vapor pressure deficit and days since rain) and with leaf area index (LAI). Analysis of 140 sites with high-quality estimates for at least two continuous years shows that  $T/ET$  variability was 1.6 times higher across sites than across years. Spatial variability of  $T/ET$  was primarily driven by vegetation and soil characteristics (e.g., crop or grass designation, minimum annual LAI, soil coarse fragment volume) rather than climatic variables such as mean/standard deviation of temperature or precipitation. Overall,  $T$  and  $T/ET$  patterns are plausible and qualitatively consistent among the different water flux partitioning methods implying a significant advance made for estimating and understanding  $T$  globally, while the magnitudes remain uncertain. Our results represent the first extensive EC data-based estimates of ecosystem  $T$  permitting a data-driven perspective on the role of plants' water use for global water and carbon cycling in a changing climate.

#### KEYWORDS

ecohydrology, eddy covariance, evaporation, evapotranspiration, FLUXNET, transpiration

## 1 | INTRODUCTION

Transpiration ( $T$ ) is the flux of water vapor and latent energy returned to the atmosphere by vascular plants, mainly through the stomatal pores on their foliage and concurrent with photosynthesis.  $T$  is thus the nexus of the terrestrial water, carbon, and energy cycles, making it a key process in the Earth System. Better understanding of  $T$  could have practical implications through better understanding of plant water use and water limitations (Allen, Breshears, & McDowell, 2015; Bernacchi & VanLoocke, 2015), understanding which can then improve water resource management and prevent economic losses (Fisher et al., 2017). However, estimating ecosystem scale  $T$  is challenging, so  $T$  is generally studied extensively in

laboratories, plant growth chambers, and greenhouses. The difficulty of estimating ecosystem  $T$  is due to heterogeneities in the physical and physiological properties and processes underlying plant water uptake and ecosystem water use (Kool et al., 2014). These challenges cause limited availability and large uncertainties in ecosystem  $T$  estimates, and this propagates to uncertainties in biosphere-atmosphere feedbacks relevant for projections of climate change by Earth System models (Fisher et al., 2017).

The eddy covariance (EC) technique has been proven to be a useful tool for measuring ecosystem water, carbon, and energy fluxes worldwide (Baldocchi, 2020). A key advantage of the EC technique is the near continuous, sub-daily sampling and the intermediate spatial scale of measurements which integrates over the ecosystem and can

be linked to remote sensing products (Chu, Baldocchi, John, Wolf, & Reichstein, 2017; Jung et al., 2011; Kumar, Hoffman, Hargrove, & Collier, 2016). EC measures aggregate fluxes, and therefore fluxes related to individual processes must be estimated using modeling and post-processing. In the case of carbon dioxide ( $\text{CO}_2$ ), net ecosystem exchange of  $\text{CO}_2$  fluxes (NEE) can be partitioned into gross primary productivity (GPP) and ecosystem respiration (Lasslop et al., 2010; Reichstein et al., 2005). Applying the  $\text{CO}_2$  partitioning methods across many sites from communities willing to collaborate (e.g., FLUXNET) has proven valuable in a wide range of contexts (Baldocchi, 2008), from model evaluation (Friend et al., 2007) to empirical upscaling of global products (Jung et al., 2011). The opportunity to replicate the success of  $\text{CO}_2$  flux partitioning with water flux partitioning has resulted in a number of methods that attempt to distinguish the physiologically regulated  $T$  flux from the measured evapotranspiration (ET) flux, which also contains abiotic evaporation ( $E$ ) from soil and canopy-intercepted water. Partitioning the existing ET from FLUXNET would improve cross site comparisons of GPP to  $T$  dynamics, which have previously relied on filtering each site for periods after rain events to minimize the effect of  $E$ .

Here we applied three recent methods for estimating  $T$  from EC datasets: the underlying water use efficiency (uWUE) method (Zhou, Yu, Zhang, Huang, & Wang, 2016), the Pérez-Priego method (Perez-Priego et al., 2018), and the Transpiration Estimation Algorithm (TEA) method (Nelson et al., 2018). We focused on methods which utilize current EC datasets, such as FLUXNET and the associated regional networks, which include continuous measurements of  $\text{CO}_2$ , sensible, and latent heat fluxes, as well as meteorological variables at half-hourly or hourly time steps. All three methods utilize GPP estimates to partition  $E$  and  $T$  from ET, as  $\text{CO}_2$  uptake and water vapor losses from  $T$  are both regulated via stomata in higher plants and are thus inherently linked (Cowan & Farquhar, 1977). Note that other ET partitioning methods exist, including methods that only use EC datasets, which are not highlighted here. Such methods include Scott and Biederman (2017), which may not be applicable at non-water-limited sites, and Li et al. (2019), which requires ancillary data such as canopy height and soil moisture. As reviewed in Anderson, Zhang, and Skaggs (2017), other methods for estimating  $T$  are being developed, such as flux variance partitioning of high frequency data using water use efficiency (WUE) measured at the leaf scale (Scanlon & Kustas, 2010; Scanlon, Schmidt, & Skaggs, 2019), measurement of isotopes (Berkelhammer et al., 2016; Wang, Good, Caylor, & Cernusak, 2012), carbonyl sulfide (Whelan et al., 2018), or concurrent below and above canopy EC measurements (Paul-Limoges et al., 2020). For a more detailed analysis of various water flux partitioning approaches, see Stoy et al. (2019).

## 1.1 | Drivers of $T$ and knowledge gaps

A key difficulty in distinguishing  $T$  from  $E$  is the fact that both fluxes are inherently the same physical process,  $E$ , with the core difference being that  $T$  is actively regulated by vegetation, for example, through

changes in stomatal conductance and/or root water uptake. One example is the effect of vapor pressure deficit (VPD), which, on the one hand, drives  $T$  and  $E$  but, on the other, causes stomatal closure in plants thus inhibiting  $T$ . Stomatal closing due to high VPD prevents excess plant water loss relative to carbon gain. As VPD increases,  $T$  losses would increase with no corresponding effect on GPP (assuming no other change in the environment, stomatal conductance, or non-stomatal limitations), resulting in a decrease in WUE ( $\text{WUE} = \text{GPP}/T$ ). This decrease in WUE has been shown to be a power function of VPD both from in situ chamber experiments (Pérez-Priego, Testi, Orgaz, & Villalobos, 2010; Villalobos, Perez-Priego, Testi, Morales, & Orgaz, 2012) and derived from theory (Medlyn et al., 2011). While this relationship has been demonstrated from GPP/ET ratios derived from EC data in rain-free periods (Zhou, Yu, Huang, & Wang, 2014, 2015), it should be clearly evident in a GPP/ $T$  product, and thus can be used as a first-order check on the  $T$  estimates.

Another expected pattern is the relationship between LAI and  $T$ /ET. Studies using site-level estimates of  $T$ /ET show a strong coupling to LAI (Wang, Good, & Caylor, 2014; Wei et al., 2017). This link between  $T$ /ET and LAI is in some respects intuitive: an LAI of zero would mean no vegetation and no  $T$ ; and increasing vegetation coverage would mean more transpiring surfaces and more shading of soil thus increasing  $T$ /ET.

However, seasonal covariation may not correspond to a causal relationship, as part of the covariation could be attributed to other seasonal patterns such as cycles in soil water availability or phenology. By modeling  $T$ /ET as a function of LAI, Wei et al. (2017) were able to capture between 43% and 87% of the variance depending on vegetation type. However, Wang et al. (2014) showed high variability of  $T$ /ET at low values of LAI, which was in part explained by plant growing stage (particularly in crops). Based on a temperate needle leaf forest site, Berkelhammer et al. (2016) reported that while LAI did match seasonal  $T$ /ET dynamics, no significant relationship was found at diel, daily, or annual timescales, indicating the LAI relationship is tied to seasonality. If LAI is a key driver of  $T$ /ET, one would expect a relationship between the two at other scales, in particular LAI should correlate with  $T$ /ET in space. Using a mechanistic ecohydrological model, Fatichi and Pappas (2017) found no relationship between mean site  $T$ /ET and LAI, rather the major driver of uncertainty was the parameterization of the hydraulic properties of the topsoil in the model. Pairing  $T$  estimates from EC and remote sensing estimates of LAI would allow for a consistent and broad-scale examination of the relationship of LAI and  $T$ /ET, and test whether the seasonal relationship observed translates to a spatial relationship indicating that LAI is a key driver of  $T$ /ET.

Aside from LAI,  $T$ /ET could be related to water availability, as plants have access to deeper soil moisture and can thus sustain a high  $T$  rate for longer periods after rain pulses. However, many studies show no relationship between  $T$ /ET and precipitation (Fatichi & Pappas, 2017; Schlesinger & Jasechko, 2014), and little relationship with water stress indicators such as soil water potential (Wang et al., 2014) or wetness index (ratio of mean precipitation to potential ET, Fatichi & Pappas, 2017). Vegetation type could also play a key role in how ET is partitioned, and indeed most previous

meta-analyses of site-level  $T/ET$  data have used some form of segregation by plant functional type (Schlesinger & Jasechko, 2014; Wang et al., 2014; Wei et al., 2017). However, these groupings tend to be imposed for data interpretation, with limited exploration into what ecosystem properties actually drive differences in ecosystem  $T/ET$ , and therefore a more in-depth analysis is warranted.

## 1.2 | Objectives

Here we present estimates of  $ET$  partitioning from three different methods across FLUXNET, providing a dataset of  $T$  estimates at ecosystem level from sub-daily to annual values and covering many climate zones and biomes. These three methods are first compared against each other to identify how well they agree. The partitioning methods are then compared to an independent data source (scaled-up sap flow measurements), both to demonstrate absolute performance and to ensure that  $T$  estimates are adding information compared to the original  $ET$  estimates. After initial assessment, we examine the  $T$  estimates for expected patterns, such as the seasonal covariation of LAI and  $T/ET$  as well as responses to dry conditions such as the expected decrease of WUE to high VPD and the increase of  $T/ET$  during dry down events. We also demonstrate the potential inadequacies of calculating WUE as  $GPP/ET$  due to  $E$ , even when filtering for rain-free days. Finally, we use full-year estimates of  $T$  and  $ET$  to explore the drivers of variability in  $T/ET$  across sites.

## 2 | METHODS

### 2.1 | EC data

Flux data from the FLUXNET2015 dataset (Pastorello et al., 2017) were used. In some cases, sites were included from the previous La Thuile dataset when not available in the FLUXNET2015 release. An overview of the variables used in this study can be found in Table S1. In all cases, GPP was estimated from the EC-measured NEE using the night time flux partitioning method (Reichstein et al., 2005).

The sites used in this study are distributed widely across the globe and they represent diverse ecosystems from a variety of climatological conditions. However, the global distribution of observations is largely biased toward Western countries in the Northern Hemisphere, with most of the sites located in USA, Western Europe, and East Asia. All sites, as well as the plant function type (PFT) designation are listed in both table and map form in File S1.

### 2.2 | ET partitioning methods

#### 2.2.1 | Descriptive overview of the $T$ partitioning methods

The  $uWUE$  method relies on estimates of the  $uWUE$ , defined as,

$$uWUE = \frac{GPP \cdot \sqrt{VPD}}{ET}, \quad (1)$$

where VPD is the vapor pressure deficit. Two  $uWUE$  variants are calculated from half-hourly data: (a) the potential  $uWUE$  ( $uWUE_p$ ) is calculated at an annual scale using a 95th percentile regression between  $GPP \cdot \sqrt{VPD}$  and  $ET$ , representing conditions with the highest carbon gain to water loss and thus  $T \approx ET$ ; (b) the apparent  $uWUE$  ( $uWUE_a$ ) is estimated as the linear regression slope from a moving window spanning either one or eight days (depending on desired smoothing and data availability), or directly from Equation (1) when estimating at half-hourly resolution.  $uWUE_p$  is assumed to be constant throughout a year, corresponding to the maximum carbon gain to water loss given that  $\sqrt{VPD}$  linearizes the  $ET$  to  $GPP$  relationship, as has been shown across a large variety of sites and has been linked to stomatal optimality (Zhou et al., 2014).  $T/ET$  is then estimated as,

$$\frac{T}{ET} = \frac{uWUE_a}{uWUE_p}. \quad (2)$$

As the method utilizes comparatively simple computations,  $uWUE_p$  and  $uWUE_a$  calculated as slopes or ratios, the  $uWUE$  method is the simplest of the three methods to calculate.

The Pérez-Priego method on the other hand utilizes a more complete “big leaf” model, where four different parameters are fit in a 5-day moving window. The fit parameters relate to the response of canopy conductance to VPD, photosynthetically active radiation, and temperature, as well as to the response of the maximum photosynthetic rate to VPD and ambient  $CO_2$ . The method also incorporates the leaf optimality concept, that is carbon gain to water loss is maximized, by integrating a penalty in the cost function for parameters that result in poor leaf carbon:water optimality. One distinctive feature of the Pérez-Priego method is that it never makes the assumption that  $T \approx ET$ .

Finally, the TEA method utilizes a nonparametric model, a version of Random Forest (Breiman, 2001), to predict WUE ( $GPP/T$ ). The model is trained on the ecosystem WUE ( $WUE_{eco} = GPP/ET$ ) during periods in the growing season and when surfaces are likely to be dry, that is, where  $E/ET$  should be minimal. Periods likely to have wet surfaces are filtered based on precipitation input and  $ET$  in a shallow bucket, water balance scheme (see Nelson et al., 2018 for a full description). The RF, trained on  $WUE_{eco}$  from the filtered periods, then predicts WUE (now  $GPP/T$ ) for the full time series. To further compensate for the existence of  $E$  in the training dataset, a higher prediction percentile of WUE is output from the RF (Meinshausen, 2006). Nelson et al. (2018) determined that the 75th percentile was the most appropriate prediction percentile based on the best performance when assessed against synthetic data from three terrestrial biosphere models. In contrast to the  $uWUE$  or Pérez-Priego methods, the TEA method utilizes a machine learning approach that allows for the predicted WUE to be dynamic in time and not strictly driven by assumed physiological responses—for example, the response of WUE to VPD comes from the data itself rather than an assumption of leaf carbon:water optimality.

In summary, the three methods are characterized by key differences in their assumptions, structure, and conceptualization: number of parameters (one or two in uWUE depending on temporal scale vs. four in Pérez-Priego), parametric versus nonparametric (uWUE and Pérez-Priego vs. TEA), the assumption that  $T \approx ET$  for some portion of the data (uWUE and TEA vs. Pérez-Priego), and the inclusion of physiological parameters describing the leaf carbon:water optimality (Pérez-Priego and uWUE vs. TEA).

## 2.2.2 | Application of $T$ methods to EC data

The uWUE method was implemented based on the published description (Zhou et al., 2016), with uWUE<sub>p</sub> estimates made for each year and uWUE<sub>a</sub> estimates derived using the 8-day moving window. The resulting Python code can be found in the associated code repository (Nelson, 2020b). The uWUE method was also estimated at half-hourly scale by directly calculating  $uWUE_a = GPP \cdot \sqrt{VPD} \cdot ET^{-1}$  (Zhou, Yu, Zhang, Huang, & Wang, 2018).

The Pérez-Priego method was implemented using an open-source R package (Perez-Priego & Wutzler, 2019). Parameter optimization was performed on a daily basis using a 5-day moving window containing high-quality data: (a) quality flags of the CO<sub>2</sub> fluxes = 0 (directly measured, non-gap-filled according to Reichstein et al., 2005); and (b) half hours with measured precipitation removed.

The TEA algorithm used code version v1.06 (Nelson, 2019), which was updated from the original published version with minor modifications to improve data filtering and include additional checks to ensure night time  $T$  fluxes were set to zero.

Though each method has been previously described in the respective publications, an in-depth tutorial for each method can be found as both an interactive and static form in the associated code repository (Nelson, 2020b). Furthermore, the data can be accessed from Nelson (2020a).

Comparison and evaluation of the methods was complicated due to differences in how the methods were applied. In particular, the estimation procedure from Pérez-Priego did not always find adequate solutions for the parameters, resulting in some erratic values of  $T$  and thus preventing continuous estimates of  $T$ , affecting on average 29% of the data across sites. Missing Pérez-Priego values due to inadequate parameters were not gap-filled, which limited the daily and monthly aggregate values of  $T$  to periods without missing data, leaving very few complete months. Due to the differences in applicability, comparisons of all three EC-based partitioning methods were limited to intercomparisons between the methods and with the sap flow data, while broader comparisons (e.g., across years or sites) were done only with the TEA and uWUE methods.

## 2.3 | Sap flow estimates

Stand  $T$  was obtained by upscaling sap flow measurements ( $T_{SF}$ ) from six forest sites in the SAPFLUXNET database (Poyatos et al., 2016)

which overlapped in time with the FLUXNET2015 dataset (Table S2). SAPFLUXNET datasets contain sub-daily sap flow rates, scaled to the tree level according to site-specific procedures, which are documented within the dataset metadata (Poyatos et al., 2019). In order to obtain stand-level  $T$ , we first temporally aggregated the data to daily sap flow values per tree (kg/day) and retained only those days with sufficient coverage (80% of the sub-daily time steps). We then normalized sap flow per unit basal area of each tree and averaged the values for each species present in the datasets. In all datasets, the species in which sap flow was measured represented >90% of the stand basal area (Table S2). The value of species-specific sap flow per basal area was multiplied by the basal area of each species in the stand and then data from all species were summed to obtain stand-level  $T$  (mm/day). All the tree and stand-level variables needed for the upscaling were extracted from the metadata corresponding to each dataset (Poyatos et al., 2019).

## 2.4 | Gridded and remote sensing data

This study utilized three different sources of remote sensing data to explore the spatial and temporal relationships between vegetation indices and  $T/ET$ . First, leaf area index (LAI) and fraction of photosynthetically active radiation (fPAR) estimates for each FLUXNET site were derived from the Joint Research Centre Two-stream Inversion Package product (Pinty et al., 2011) and summarized for each site using the mean, minimum, maximum, standard deviation, and the 95th and 99th percentiles. Furthermore, the entire multi-temporal Collection 1 from the Landsat 4, 5, 7, and 8 archives (<https://www.usgs.gov/>) was collected. The blue, red, near-infrared, and shortwave infrared spectral bands (<https://landsat.usgs.gov/what-are-band-designations-landsat-satellites>) were retrieved to compute normalized difference vegetation index (NDVI; Tucker, 1979), enhanced vegetation index (EVI; Huete et al., 2002), and normalized difference water index (NDWI; Jin & Sader, 2005). Low-quality Landsat pixels due to clouds, cloud shadows, snow, and ice were masked out (Zhu, Wang, & Woodcock, 2015; Zhu & Woodcock, 2012). Finally, 4 day values (as the best pixel from a 4 day window) of LAI from the MCD15A3H version 6 MODIS product (Myneni & Knyazikhin, 2015) were used to analyze the relationship of LAI to  $T/ET$  (Figure 3). The quality layer for LAI (i.e., FparLai\_QC) of the MCD15A3H version 6 product was used for filtering out low-quality observations (i.e., cloudy pixels and pixels covered with snow/ice were discarded). For both Landsat and MODIS products, the data extraction and the preprocessing chains (i.e., cloud, cloud shadow masking, and downloading) were implemented in the Google Earth Engine platform (Gorelick et al., 2017; <https://earthengine.google.com/>). Landsat (i.e., NDVI, EVI, and NDWI) and MODIS (i.e., MCD15A3H LAI) data were summarized for each site using the mean and 95th percentiles.

Additionally as spatial covariates of  $T/ET$ , five soil properties for each site were estimated using the SOILGRIDS dataset (Hengl et al., 2017): coarse fragment volume, soil pH, and percent of clay, sand, and silt. Soil properties were summarized for each site using a weighted mean for the full depth available. In all cases, spatial data

were aggregated from an area within  $\approx 1$  km of the tower location by taking the mean for all good quality pixels in the selected area.

## 2.5 | Spatial modeling of $T/ET$ and variable importance

To infer potential drivers of the spatial variability of  $T/ET$ , 44 different variables composed of estimated soil properties, vegetation indices from remote sensing, plant functional type classifications, and climate variables measured on site were used to predict site average annual  $T/ET$  (one value per site) using a Random Forest model (Breiman, 2001). Variables were preselected using the approach of Jung and Zscheischler (2013), which attempts to maximize the model performance while minimizing the required number of variables. Variable selection was repeated 10 times and all resulting models were compared to select the top performing feature set. Furthermore, feature importance was estimated by examining the selection frequency of each variable, with the assumption that important features will be selected often in top performing models, while less important features will be selected infrequently. The selection frequencies of the 10 independent feature selection runs were then summarized as a mean and standard deviation.

## 3 | RESULTS

### 3.1 | Intercomparison of the ET partitioning methods

In general, all three methods agreed with respect to overall patterns, with the lowest correlation (Spearman,  $R_{sp}$ ) of daily  $T$  found between uWUE and Pérez-Priego ( $R_{sp} = .89$ ) and the highest between uWUE and TEA ( $R_{sp} = .94$ ). For context, the correlations between  $T$  from the three methods and ET ranged from  $R_{sp}$  of .71 to .82. The magnitude (daily sum) of  $T_{TEA}$  was much higher than those of the other two methods, with  $T_{uWUE}$  and  $T_{Pérez-Priego}$  being 68% and 58% of  $T_{TEA}$ , respectively, across all sites. Figure 1 shows an intercomparison of the three methods at daily resolution. Note that the results presented here used the night time partitioning method to estimate GPP (Reichstein et al., 2005), which is highly consistent with  $T$  estimates from the day time partitioned GPP (Lasslop et al., 2010; Figure S1).

### 3.2 | Evaluation with sap flow $T$ estimates

As an independent evaluation, all three EC-based  $T$  estimates were compared to the estimates of stand  $T$  computed from sap flow sensors ( $T_{SF}$ ) at six different forest sites at daily resolution. Overall, the EC-based  $T$  estimates had a higher correlation with  $T_{SF}$  compared to total ET from EC, with correlations averaging 0.81, 0.78, and 0.76 for  $T_{TEA}$ ,  $T_{Pérez-Priego}$ , and  $T_{uWUE}$ , respectively,

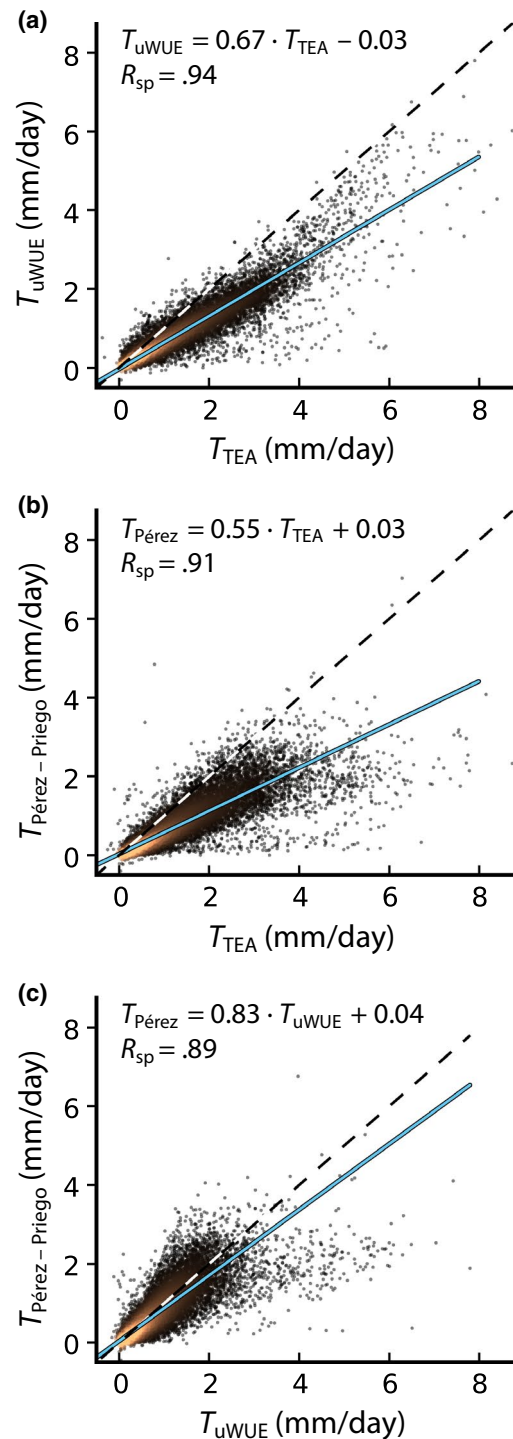


**FIGURE 1** Intercomparison of the three transpiration ( $T$ ) estimation methods presented here at daily resolution comparing  $T_{TEA}$  to  $T_{uWUE}$  (a),  $T_{TEA}$  to  $T_{Pérez-Priego}$  (b) and  $T_{uWUE}$  to  $T_{Pérez-Priego}$  (c). Points ( $n = 53,390$  from 127 sites) come from the intersection of all methods where  $T$  could be estimated.  $R_{sp}$  values correspond to Spearman rank correlations to reduce the influence of outliers. Linear equation was estimated using orthogonal-least-squares regression which assumes observational errors exist in both  $x$  and  $y$ . Dark to light point coloration corresponds to low to high relative point density, respectively

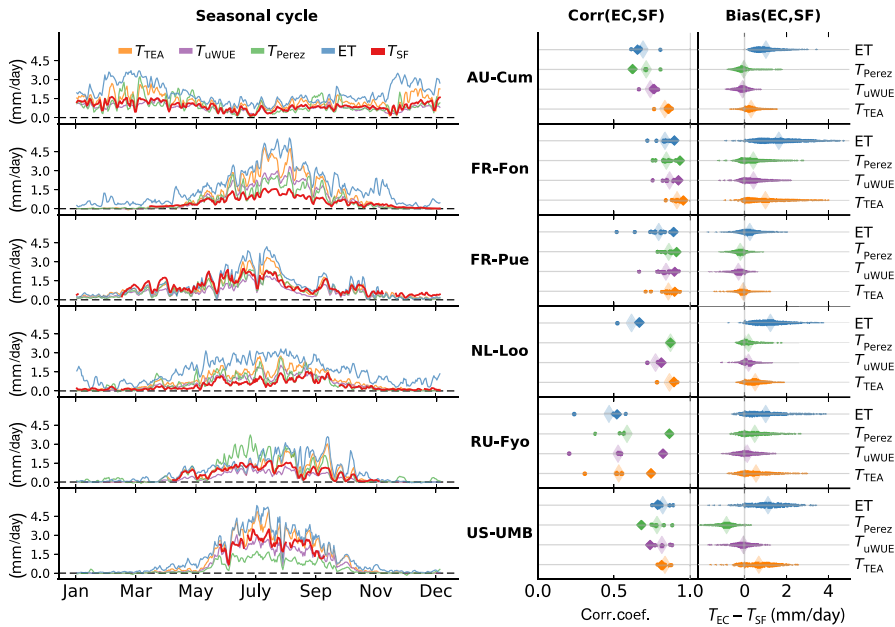


**FIGURE 2** Comparison of sap flow-based estimates of transpiration ( $T_{SF}$ ) against estimated transpiration ( $T$ ) and measured evapotranspiration (ET) from eddy covariance (EC). Note the three different sizes of markers in the correlation plots ( $\text{corr}(\text{EC}, \text{SF})$ , Pearson correlation), where the largest markers represent the mean correlation, the smallest markers represent the correlations from each available year, and the medium-sized markers represent the selected year shown (time series in the left column of sub-figures)

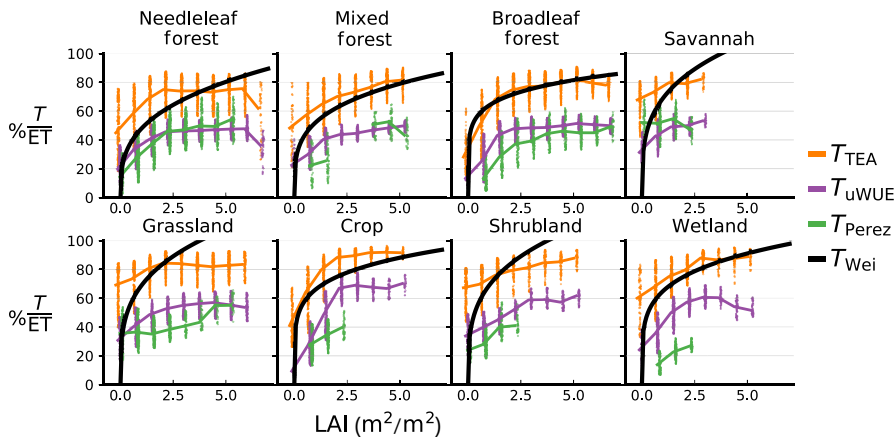


**FIGURE 3** Daily transpiration ( $T$ )/evapotranspiration (ET) from each EC-based method as a function of MODIS LAI. For each plant function type (PFT), the associated relationship derived from Wei et al. (2017) is shown in black, which was derived from site-level  $T/\text{ET}$  estimates. Points show the distribution within the given LAI bin, truncated to the 25th and 75th percentiles. PFTs were grouped to match those found in Wei et al. (2017) and are slightly different compared to subsequent figures

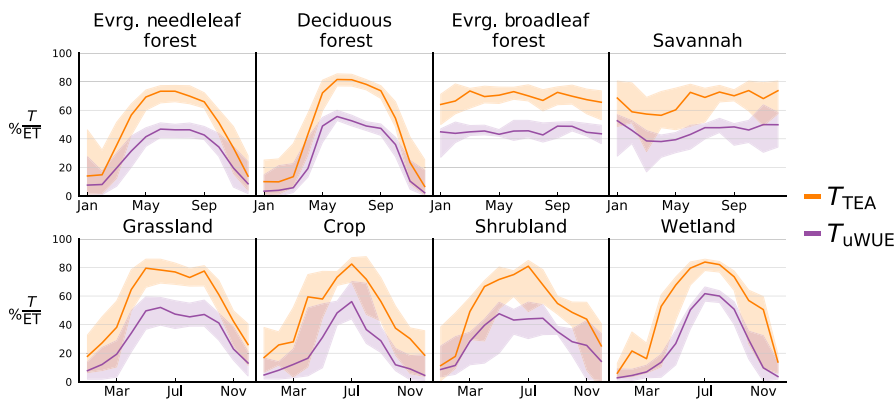


**FIGURE 4** Mean monthly seasonal cycles of transpiration ( $T$ )/evapotranspiration (ET) grouped by plant function type (PFT) from the Transpiration Estimation Algorithm and underlying water use efficiency methods. Mean seasonal cycles for each site are grouped by PFT, with lines indicating the median across sites and shading indicating the interquartile range. Note that data from sites in the Southern Hemisphere have been shifted by 6 months, for example January in the figure would correspond to July in a Southern Hemisphere site

compared to 0.70 for ET (Figure 2). The bias between  $T$  from the EC partitioning methods and  $T_{SF}$  ( $T_{EC} - T_{SF}$ ) was smaller compared to the bias between ET and  $T_{SF}$ , with site root mean square error between 0.33–1.36, 0.28–0.67, and 0.36–0.96 mm/day for the TEA, uWUE, and Pérez-Priego methods, respectively, compared to 0.53–1.95 mm/day for ET.

### 3.3 | $T/\text{ET}$ patterns with LAI and seasonality

Figure 3 shows the relationship of  $T/\text{ET}$  across the FLUXNET dataset for each method compared to LAI derived from MODIS, grouped into eight PFTs. Additionally, a line is shown describing the relationship between  $T/\text{ET}$  and LAI derived from Wei et al. (2017), where



non-EC-based  $T/ET$  estimates were used to derive parameters  $a$  and  $b$  in the model,

$$\frac{T}{ET} = a \cdot e^{b \cdot LAI}. \quad (3)$$

The estimates of  $a$  and  $b$  per PFT were taken from Wei et al. (2017) to calculate the  $T/ET$  response to LAI shown (Wei method). Compared to the Wei method, the EC-based methods showed a more gradual decline in  $T/ET$  as LAI approaches zero, with the exception of ecosystems dominated by deciduous vegetation, that is, crops and temperate broad-leaved forests. At LAI values above  $1 \text{ m}^2/\text{m}^2$ , the higher  $T/ET$  values from the TEA method were more consistent with the Wei method, with the uWUE and Pérez-Priego estimated  $T/ET$  being significantly lower. Note that the curves from the Wei method are based on site LAI estimates, whereas the data in Figure 3 were derived from remote sensing-based LAI which may not reflect what was seen by the EC systems.

Utilizing the fact that the TEA and uWUE methods could be successfully applied at most FLUXNET sites, Figure 4 gives an overview of the mean seasonal cycle of  $T/ET$  for eight PFTs. Overall, the seasonal patterns of  $T/ET$  are largely consistent between the two methods, showing larger  $T/ET$  during the growing season as expected. The differences in magnitude are immediately clear for the TEA and uWUE methods, with peak seasonal  $T/ET$  being on average 83% and 58%, respectively. Interestingly, both methods showed a relatively consistent peak season  $T/ET$  value across all PFTs, even between PFTs dominated by different climates, for example, similar max  $T/ET$  between evergreen broad-leaf forests which are primarily in tropical and subtropical regions and evergreen needleleaf forests which are primarily located in temperate regions. Note that the PFT groupings in Figure 4 were selected to better capture both differences in plant function and biomes, such as separating deciduous forests from evergreen broadleaf forests, and are slightly different from those in Figure 3 which correspond to the groupings from Wei et al. (2017).

### 3.4 | WUE and $T/ET$ patterns with VPD

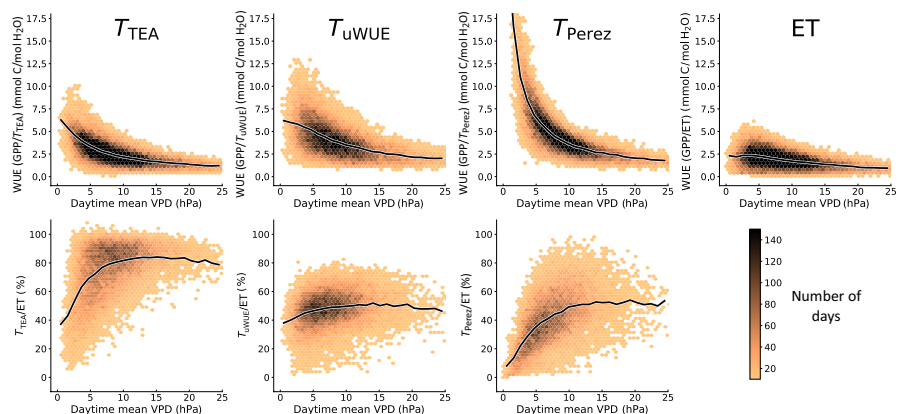
Figure 5 shows the exponential-type relationship of WUE (GPP/ $T$ ) to VPD for the TEA, uWUE, and Pérez-Priego methods

across all sites where  $T$  could be estimated by all the methods. In contrast, a similar decay was not evident for WUE computed as GPP/ $ET$ , lacking the distinctive rise as VPD approaches zero. The reason why the GPP/ $ET$  relationship does not exponentially rise as VPD approaches zero is due to a sharp decrease in  $T/ET$  at low VPD (Figure 5). In other words, as VPD decreases,  $T/ET$  also decreases, likely due to the fact that periods of low VPD correspond to periods after rain or dewfall when surfaces are wet and the  $E$  component of  $ET$  is relatively high. Consequently, the higher  $E/ET$  proportion masked the physiological effect of enhanced WUE at low VPD conditions, highlighting the conceptual bias of  $ET$ -based WUE estimates and the added value of  $ET$  partitioning.

### 3.5 | Remaining evaporation in consecutive rain-free days

Previous studies used  $ET$  as a proxy for  $T$  by filtering for periods after rain events with the assumption that  $T$  will dominate  $ET$ ; for example, assuming that  $E$  will become negligible after 3 days with no significant rain (e.g., Knauer et al., 2018). To test this hypothesis, we estimated  $E/ET$  (where  $E = ET - T$ ) across all possible sites and grouped into periods of 0–5 or more consecutive days after rain, both at the daily and sub-daily scales (Figure 6). In the case of daily resolution,  $E$  estimates from all three methods show declining  $E/ET$  over the first three consecutive rain-free days. However, no method showed zero  $E$ , instead falling to 50%, 44%, and 16% average  $E/ET$  after five or more days after rain for Pérez-Priego, uWUE, and TEA, respectively. Though daily  $E/ET$  did not fall to zero, the diurnal cycles from all methods indicated periods during the day when  $E/ET$  is zero. These diurnal cycles showed contrasting patterns. Both the TEA and Pérez-Priego methods showed a tendency for higher  $E/ET$  in the morning compared to afternoon, with the pattern being much more prominent for the Pérez-Priego method where it persists even after 5 days without rain, whereas the pattern almost disappears for TEA under drier conditions. The uWUE method consistently showed a peak in  $E/ET$  during the afternoon, with the lowest  $E/ET$  in the morning hours.

**FIGURE 5** Relationship of both water use efficiency (top row) and transpiration ( $T$ )/evapotranspiration ( $ET$ ; bottom row) to day time mean vapor pressure deficit at daily scale across 124 sites. Lines indicate the median value from 1 hPa wide bins. Only days with a mean temperature above  $5^\circ\text{C}$ , at least 1 mm/day of  $ET$ , and where all three partitioning methods could be applied were included



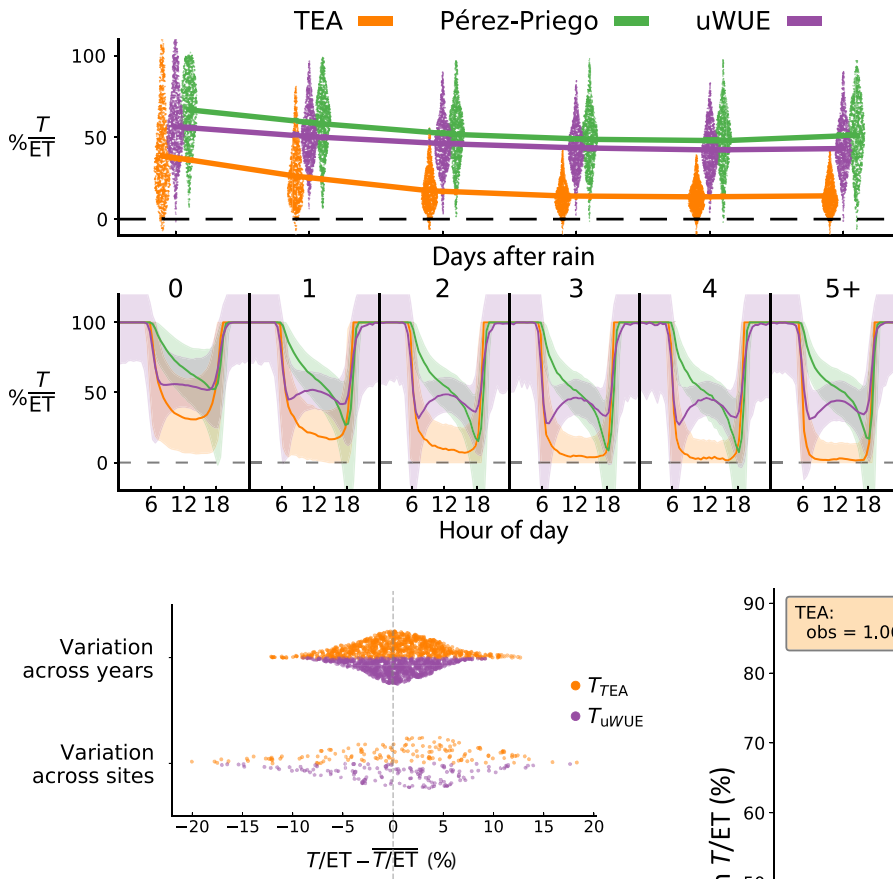


**FIGURE 7** Comparison of variability of transpiration ( $T$ )/evapotranspiration ( $ET$ ) across years and across sites. Variability across years was calculated as the  $T/ET$  for each year of one site minus the mean across years from that site (only sites with at least 2 years of data). Each point refers to a site and the vertical spread indicates the distribution of points (the underlying water use efficiency [uWUE] method is mirrored for better comparability). Variability across sites was calculated as the mean  $T/ET$  for each site minus the mean across all 140 sites. Overall, the standard deviations across sites were 1.6 and 1.5 times the standard deviations across years (for the uWUE and Transpiration Estimation Algorithm methods, respectively)

### 3.6 | Patterns of between-site $T/ET$ variability

Perhaps the most significant advantage of the widely applicable  $T$  estimations is the possibility to make complete annual estimates of  $T$ , as they permit the comparison of interannual and across site  $T$  and  $T/ET$  variability. As seen in Figure 7,  $T_{TEA}/ET$  and  $T_{uWUE}/ET$  both showed 60% higher variability (standard deviation) between sites than between years (mean of TEA and uWUE). In other words,  $T/ET$  was much more different from one site to another compared to from different years of the same site. This higher spatial variability would suggest that annual  $T/ET$  was more related to site characteristics than to the year-to-year changes in environmental conditions. Figure 8 shows the model performance of a Random Forest model for predicting site  $T/ET$  for both TEA- and uWUE-based estimates. The models had Nash-Sutcliffe efficiencies (NSE, Nash & Sutcliffe, 1970) of 0.44 and 0.43 for TEA and uWUE, respectively. Overall, the model tended to deflate the variance in site  $T/ET$

**FIGURE 6** Percentage of evaporation ( $E/ET$ ) estimated using the Transpiration Estimation Algorithm, underlying water use efficiency, and Pérez-Priego methods for progressive days after rain (rainy days defined as receiving  $>0.1$  mm in 1 day). Upper and lower panels show daily aggregated and diurnal cycles of  $E/ET$ , respectively. Diurnal cycles are estimated as the median for each half hour, with the interquartile range shown as shading. Only days with a mean temperature above  $5^{\circ}\text{C}$ , at least 1 mm/day of  $ET$ , and where all partitioning methods could be applied for all half hours in a day were included

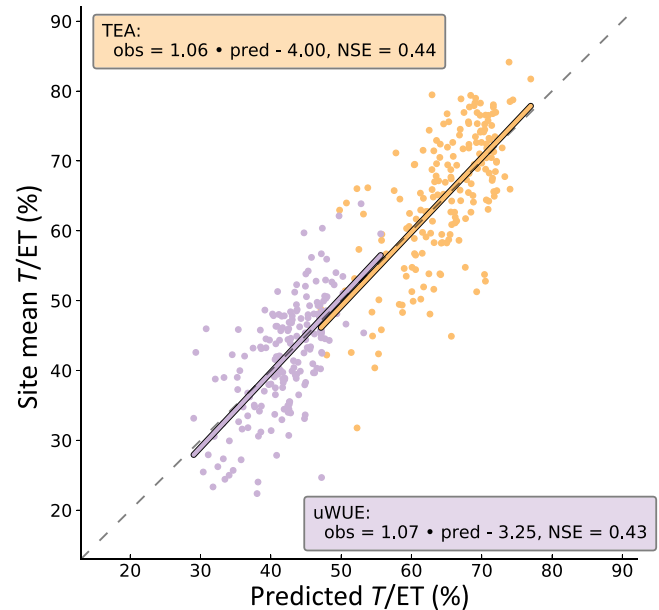


**FIGURE 8** Evaluation of the performance of the Random Forest model according to the amount of spatial variability explained across sites. Predicted values are from the out of bag estimates of transpiration/evapotranspiration, that is estimates from the Random Forest model that do not use the corresponding point being predicted. Features used in this model were: grassland designation, crop designation, soil pH, min. MODIS LAI, % sand, mean MODIS EVI, mean LANDSAT NDMI, coarse fragment vol

$ET$ , indicating an incomplete variable set. Figure 9 shows an estimate of variable importance based on how often each variable was selected in the best models (all models with  $NSE > NSE_{\max} - 0.05$ ). The five most frequently chosen variables were cropland designation, minimum LAI, soil coarse fragment volume, grassland designation, and soil percent silt content, followed by a number of vegetation indices. Interestingly, most meteorological variables, which were the only variables actually measured at site level, were rarely selected, with mean and standard deviation of annual precipitation never being selected in the best models.

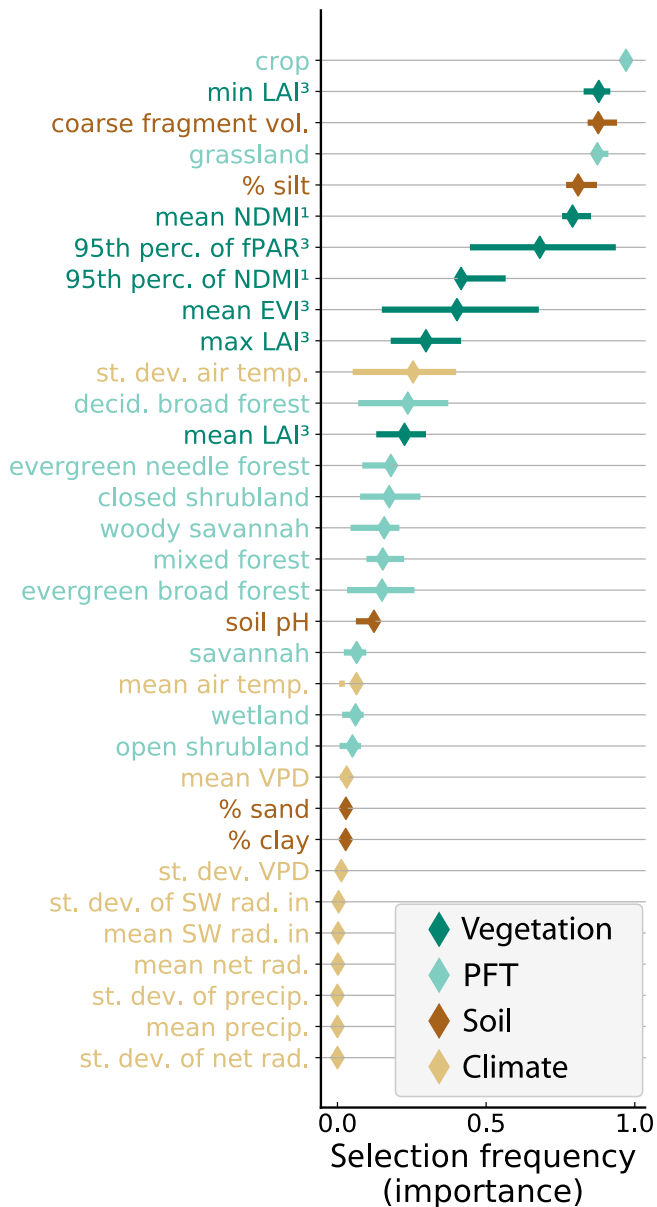


**FIGURE 9** Selection frequency, or how often each variable was selected during feature selection, gives an indication of variable importance. Points represent the median selection frequency from 10 iterations of feature selection, with the interquartile range shown as error bars. Remote sensing-derived variables come from either <sup>1</sup>LANDSAT, <sup>2</sup>TIP, or <sup>3</sup>MODIS (see Section 2 for a full description). Plant function type designations are site reported. Climate data come from site measurements. Soil data were derived from the SOILGRIDS dataset (Hengl et al., 2017)

## 4 | DISCUSSION

### 4.1 | Assessment of EC-based *T* estimates and their added value over ET

*T*/ET estimates from the TEA, uWUE, and Pérez-Priego methods across FLUXNET showed overall consistent patterns; for example, with respect to LAI, VPD, and seasonality. Furthermore, *T* from the

partitioning methods, when compared to ET, showed higher correlation with the measured and upscaled sap flow data (Figure 2) and a more physiologically plausible WUE response to VPD (Figure 5), indicating that *T* from the partitioning methods better represents the true plant physiology-driven *T* than the bulk flux (ET). Indeed, ET may not be an adequate approximation of *T* even 5 days after rain (Figure 6). This may have implications in the larger than theoretically expected increases in WUE as a result of increasing atmospheric CO<sub>2</sub> concentration (Keenan et al., 2013) or the discrepancy between leaf and ecosystem WUE (Medlyn et al., 2017), both of which were previously estimated using ET from periods 2 or more days after rain.

Though the patterns of *T* seemed to agree well between the methods, it is obvious that there still persists a large spread in the magnitude of the estimated *T*/ET (Figure 3). *T*/ET estimates from the uWUE and Pérez-Priego methods were smaller and more similar in magnitude (*T*/ET = 52% and 45%, respectively, calculated as a slope of daily *T* and ET) compared to values from the TEA method (*T*/ET = 77%). Though the magnitude of *T*/ET is difficult to estimate over broad scales, Schlesinger and Jasechko (2014) estimated 67%, 57%, and 55% mean *T*/ET for temperate deciduous forests, temperate grasslands, and temperate coniferous forests, respectively, which was closer to the TEA method (70%, 67%, and 62%) compared to the uWUE method (45%, 43%, and 40%).

One potential limitation of all three methods is that they use a GPP estimate, and are thus tied to the biases and uncertainties of the NEE partitioning methods. However, Figure S1 shows that, when comparing *T* estimated from both night time (Reichstein et al., 2005) and day time (Lasslop et al., 2010) based GPP, the resulting two *T* estimates have a higher correlation than the two GPP products do to each other. In other words, *T* estimates are consistent even when the underlying GPP estimate has changed. This is likely due both to averaging aspects of the methods (e.g., parameters estimated in moving windows in the uWUE and Pérez-Priego methods) and that GPP is not directly used (e.g., Pérez-Priego calculates *T* from stomatal conductance and VPD) or canceled out in the final step of *T* estimation (e.g., TEA estimates *T* as GPP divided by predicted WUE thus canceling out GPP, i.e.,  $T = GPP (GPP/T)^{-1}$ , similar for uWUE). However, systematic biases in GPP and ET can affect the ET partitioning methods in different ways. For example, Figure S3 shows the response of the estimated *T* after applying each method to a dataset with manipulations to either GPP or ET fluxes. In short, the Pérez-Priego method is directly affected by major changes or errors in GPP, but is independent of ET. In contrast, both the uWUE and TEA methods are robust to systematic errors in GPP; for example, a unit conversion error which doubled GPP would have no effect on the estimated *T* from either method. Short-term errors, such as if either GPP or ET was erroneously doubled for only 1 or 2 weeks, can significantly affect TEA and uWUE. In general, uWUE is more sensitive to short-term errors in GPP, and TEA is more sensitive to short-term errors in ET. Errors in

the peak growing season have the highest impact on estimated  $T$ . Aside from GPP and ET, all three  $T$  estimation methods integrate many measurements and therefore require not only high EC measurements, but also high-quality radiation, temperature, humidity, wind, and precipitation data.

## 4.2 | Differences between the methods

The TEA and uWUE methods are the more conceptually similar of the three methods, yet they differ in two key ways. First, the TEA method estimates WUE using a nonparametric model allowing WUE to change seasonally and diurnally, whereas the uWUE method models WUE as only varying with  $\sqrt{\text{VPD}}$  within a single year. This distinction in how the two methods model WUE likely explains the differences seen in mean seasonal (Figure 4) and diurnal (Figure 6) patterns. Second, while both methods use a form of quantile prediction, the uWUE method predicts the potential WUE (uWUE<sub>p</sub>) using the 95th percentile where  $\text{GPP} \cdot \sqrt{\text{VPD}}$  is maximum relative to ET. In contrast, the TEA method uses the 75th percentile based on previous modeling experiments (Nelson et al., 2018) and assumes that while higher values of the predicted distribution more accurately reflect the true WUE, the highest prediction percentiles may overestimate WUE and thus underestimate  $T$ . This second difference is the primary cause for large difference in magnitudes, and when the 90th or 95th prediction percentiles from TEA are used, the resulting  $T$  estimates are of similar magnitude to the uWUE-based  $T$  estimates with minimal change in temporal correlation between the two (Figure S2). Therefore, the magnitude of  $T$  from both the TEA and uWUE methods is still uncertain to some degree, with TEA being more consistent with the Wei method (Figure 3) and uWUE more consistent with the sap flow-based  $T$  (Figure 2). As demonstrated for the TEA and uWUE methods, uncertainty of the magnitudes of  $T$  is determined by the design and implementation of partitioning algorithms.

Until independent estimates of  $T$  become more abundant and the models can be better constrained, the remaining uncertainty in magnitude should be acknowledged when using these methods. While many new methods for independently estimating  $T$  at ecosystem scale are being developed, sap flow-based methods will likely be one of the key tools in the near future. However, validation studies have raised concerns about the potential biases incurred by most sap flow methods (Flo, Martínez-Vilalta, Steppe, Schuldt, & Poyatos, 2019; Steppe, De Pauw, Doody, & Teskey, 2010) and additional uncertainty remains from upscaling from sap flow sensors to trees and to stands (Čermák, Kučera, & Nadezhdina, 2004; Oren, Phillips, Katul, Ewers, & Pataki, 1998). Sap flow upscaled to the ecosystem also includes only canopy  $T$  rather than both canopy and understory  $T$ , which is captured with an EC system (Blanken et al., 1997). All of these issues could contribute to the differences in magnitude between SF and EC, suggesting that neither measurement technique should be considered the best reference in all cases when it comes to the magnitude of ecosystem  $T$ . Nevertheless, sap

flow measurements offers reasonable temporal patterns of canopy  $T$ , and sap flow-derived  $T$  has often compared well with independent measurements (Flo et al., 2019; McCulloh et al., 2007) and with ET at larger scales (Wilson, Hanson, Mulholland, Baldocchi, & Wullschlegel, 2001).

Another key difference between the three methods is in assumptions on the optimality response of stomata to maximize carbon gain to water loss. The Pérez-Priego method explicitly incorporates optimality via an additional term in the cost function which penalizes suboptimal parameter sets. The uWUE method also incorporates the concept of optimality, both in the  $\sqrt{\text{VPD}}$  relationship of GPP to  $T$  which mirrors theoretical frameworks based on the optimality concept (Medlyn et al., 2011) and implicitly by the use of the 95th percentile when calculating uWUE<sub>p</sub>, which was intended to find periods where  $T \approx \text{ET}$  but also has the consequence of maximizing carbon gain to water loss. However, the resulting low values of  $T/\text{ET}$  from both methods (mean site  $T_{\text{uWUE}}/\text{ET} = 42\%$ , with the Pérez-Priego method presumably lower, compared to 65% for the TEA method) runs counter to the current consensus from site level and isotope estimates that  $T$  is the dominant terrestrial water flux (Schlesinger & Jasechko, 2014; Wei et al., 2017). Though global estimates still contain uncertainties, such as the limited number of ground studies (64 in Wei et al., 2017 and 81 in Schlesinger & Jasechko, 2014) and uncertainties in  $T/\text{ET}$  ratios estimated by global isotope studies (Coenders-Gerrits et al., 2014), the low  $T/\text{ET}$  estimated by the uWUE and Pérez-Priego methods indicates that how optimality is understood and implemented in these methods may need to be refined, such as including hydraulic (Eller et al., 2018; Sperry et al., 2017) and/or non-stomatal limitations (De Kauwe et al., 2019).

## 4.3 | Emergent spatial patterns of ecosystem $T/\text{ET}$

A large portion of the variability in  $T$  and ET are both driven by climatic drivers, particularly the available energy and atmospheric capacity to drive the evaporative process. Therefore, because much of these climatic effects cancel out when looking at  $T/\text{ET}$ , it makes sense that climate shows little control over across site variation (Figure 9). This lack of control of  $T/\text{ET}$  from climate, particularly the limited role of annual precipitation, is consistent with previous findings (Fatichi & Pappas, 2017; Paschalis, Fatichi, Pappas, & Or, 2018; Schlesinger & Jasechko, 2014). Aside from the limited control from climate, the relative stability of  $T/\text{ET}$  across sites can be explained by two hypotheses: (a) the effects of interception and soil  $E$  largely cancel each other out with regard to increasing vegetation cover (Good, Moore, & Miralles, 2017), and (b) ecosystems tend to adapt to utilize the water resources available. In the case of the first hypothesis, energy limited ecosystems with higher LAI would also have an increased interception pool, whereas water limited ecosystems may have smaller interception pools but more  $E$  coming from the soil. So both dense and sparse canopies will lead to lower

$T/ET$  with a maximum somewhere in between. The second hypothesis would suggest that plants adapted to dry ecosystems would incorporate water-saving strategies leading to improved utilization of the limited precipitation, thus increasing  $T/ET$ . The combination of these two hypotheses possibly accounts for the  $T/ET$  ratio being relatively conserved across very different ecosystems. However, both the mean and 95th percentile of NDMI did show high importance in predicting site  $T/ET$ , indicating that water stress may influence  $T/ET$ , which is consistent with previous findings (Fatichi & Pappas, 2017).

The high values of  $T/ET$  at low LAI seen in Figure 3 and consistent with Wang et al. (2014), along with the limited importance of mean or maximum LAI in predicting site  $T/ET$  (Figure 9), would indicate that  $T/ET$  may be less sensitive to LAI than previously assumed, particularly in space. However, many land surface and remote sensing-based models formulate ET partitioning in part as a function of vegetation structure such as fraction of vegetation or LAI (Lian et al., 2018; Talsma et al., 2018). Care should be taken not to equate the presence of vegetation to high  $T/ET$ . However, as seen in Figure 8, much of the variance in  $T/ET$  remains unexplained, meaning that the current set of covariates was either not representative of the EC data (i.e., spatial mismatch between satellite data and EC footprint climatology; Cescatti et al., 2012) and/or some important drivers of ecosystem  $T/ET$  may not have been included, such as temporal dynamics, crop type, forest age, or disturbance history.

#### 4.4 | Outlook

We demonstrated the progress made in estimating  $T$  from EC measured bulk ET by three complementary partitioning methods. Both tests against independent sap flow-based estimates, and the overall consistency of  $T$  and  $T/ET$  patterns among methods suggests an important step forward in estimating plant water use at ecosystem scale. The added value of  $T$  estimates compared to bulk ET is clearly evident, particularly for assessing ecophysiological more meaningful WUE patterns along atmospheric (VPD) and soil dryness gradients. Previous studies assessing WUE based on flux tower data assumed negligible daily  $E$  after a few consecutive rain-free days. Our results suggest that this assumption may be inadequate, implying that those studies may be revisited with ecosystem  $T$  estimates which may help in reconciling apparent contradictions with leaf-level estimates and theory.

Of course, the key limitation of the methods is that the magnitude of  $T$  is still left unconstrained, with the magnitude of  $T$  being tied to assumptions on how water loss to carbon gain is optimized. While the uWUE and Pérez-Priego methods tend to increase WUE giving a higher carbon gain to water loss, the resulting  $T/ET$  tends to be lower than the global consensus. However, care should be taken not to assume a method which results in a  $T/ET$  value close to the current estimates of  $\approx 60\%$  constitutes an accurate method, as current global  $T$  data are still uncertain.

In addition to the unconstrained magnitudes, discrepancies of diurnal  $T/ET$  patterns from the different flux partitioning methods further indicate a lack of theoretical and data constraints for diurnal water-carbon coupling, emphasizing the need for further studies and a better understanding of this aspect. Increased abundance and higher availability of concurrent sap flow and EC measurements allowing comparisons will help to improve flux partitioning methods. This is contingent on continued efforts to evaluate and reduce uncertainties connected with upscaling of tree sap flow measurements to ecosystem  $T$ , for example, due to the omission of the understory. To facilitate corroborations with independent large-scale  $T$  constraints from isotopes, a next step is to upscale the ecosystem  $T$  estimates from flux towers to the globe as was previously done with carbon and energy fluxes. This further opens the doors of assessing cross-consistencies with process-based land surface model simulations and remote sensing-based approaches, particularly with respect to the unexpectedly low sensitivity of  $T/ET$  spatial variation with climate and LAI across FLUXNET sites found here.












#### ACKNOWLEDGEMENTS

We acknowledge insightful discussions with Dario Papale and apologize for having a cappuccino after lunch. We further acknowledge Ulrich Weber for preparing the cappuccino. M.G. acknowledges funding by Swiss National Science Foundation project ICOS-CH Phase 2 20FI20\_173691. L.Š. was supported by the Ministry of Education, Youth and Sports of the Czech Republic within the CzeCOS program, grant number LM2015061, and by SustES-Adaptation strategies for sustainable ecosystem services and food security under adverse environmental conditions (CZ.02.1.01/0.0/0.0/16\_019/0000797). G.W. acknowledges support by the Austrian National Science Fund (FWF, project I03859) and the Province of South Tyrol ("Cycling of carbon and water in mountain ecosystems under changing climate and land use"). R.P. was supported by grants CGL2014-55883-JIN, RTI2018-095297-J-I00 (Spain), and by a Humboldt Research Fellowship for Experienced Researchers (Germany). This work used eddy covariance data acquired and shared by the FLUXNET community, including these networks: Ameri-Flux, AfriFlux, AsiaFlux, CarboAfrica, CarboEuropeIP, CarboItaly, CarboMont, ChinaFlux, Fluxnet-Canada, GreenGrass, ICOS, KoFlux, LBA, NECC, OzFlux-TERN, TCOS-Siberia, and USCCC. The ERA-Interim reanalysis data are provided by ECMWF and processed by LSCE. The FLUXNET eddy covariance data processing and harmonization was carried out by the European Fluxes Database Cluster, AmeriFlux Management Project, and Fluxdata project of FLUXNET, with the support of CDIAC and ICOS Ecosystem Thematic Center, and the OzFlux, ChinaFlux, and AsiaFlux offices. Open access funding enabled and organized by Projekt DEAL.

#### DATA AVAILABILITY STATEMENT

Data that support the findings of this study are openly available from Zenodo <http://doi.org/10.5281/ZENODO.3921923>. Furthermore, a tutorial of how to produce the  $T$  estimates can be found in the associated repository at <https://github.com/jnelson18/ecosystem-transpiration>.

## ORCID

- Jacob A. Nelson  <https://orcid.org/0000-0002-4663-2420>  
 Rafael Poyatos  <https://orcid.org/0000-0003-0521-2523>  
 Yao Zhang  <https://orcid.org/0000-0002-7468-2409>  
 Beniamino Gioli  <https://orcid.org/0000-0001-7631-2623>  
 Kathrin Fuchs  <https://orcid.org/0000-0003-1776-283X>  
 Leonardo Montagnani  <https://orcid.org/0000-0003-2957-9071>  
 Nicolas Delpierre  <https://orcid.org/0000-0003-0906-9402>  
 Luca Beletti Marchesini  <https://orcid.org/0000-0001-8408-4675>  
 Damiano Gianelle  <https://orcid.org/0000-0001-7697-5793>  
 Ladislav Šigut  <https://orcid.org/0000-0003-1951-4100>  
 Simon Besnard  <https://orcid.org/0000-0002-1137-103X>

## REFERENCES

- Allen, C. D., Breshears, D. D., & McDowell, N. G. (2015). On underestimation of global vulnerability to tree mortality and forest die-off from hotter drought in the Anthropocene. *Ecosphere*, 6(8), art129. <https://doi.org/10.1890/ES15-00203.1>
- Anderson, R. G., Zhang, X., & Skaggs, T. H. (2017). Measurement and partitioning of evapotranspiration for application to vadose zone studies. *Vadose Zone Journal*, 16(13), 1–9. <https://doi.org/10.2136/vzj2017.08.0155>
- Baldocchi, D. (2008). 'Breathing' of the terrestrial biosphere: Lessons learned from a global network of carbon dioxide flux measurement systems. *Australian Journal of Botany*, 56(1), 1. <https://doi.org/10.1071/BT07151>
- Baldocchi, D. D. (2020). How eddy covariance flux measurements have contributed to our understanding of *Global Change Biology*. *Global Change Biology*, 26, 242–260. <https://doi.org/10.1111/gcb.14807>
- Berkelhammer, M., Noone, D. C., Wong, T. E., Burns, S. P., Knowles, J. F., Kaushik, A., ... Williams, M. W. (2016). Convergent approaches to determine an ecosystem's transpiration fraction: Transpiration fraction of two forests. *Global Biogeochemical Cycles*, 30(6), 933–951. <https://doi.org/10.1002/2016GB005392>
- Bernacchi, C. J., & VanLoocke, A. (2015). Terrestrial ecosystems in a changing environment: A dominant role for water. *Annual Review of Plant Biology*, 66(1), 599–622. <https://doi.org/10.1146/annurev-arplant-043014-114834>
- Blanken, P. D., Black, T. A., Yang, P. C., Neumann, H. H., Nesic, Z., Staebler, R., ... Lee, X. (1997). Energy balance and canopy conductance of a boreal aspen forest: Partitioning overstory and understory components. *Journal of Geophysical Research: Atmospheres*, 102(D24), 28915–28927.
- Breiman, L. (2001). Random forests. *Machine Learning*, 45(1), 5–32.
- Čermák, J., Kučera, J., & Nadezhdina, N. (2004). Sap flow measurements with some thermodynamic methods, flow integration within trees and scaling up from sample trees to entire forest stands. *Trees*, 18(5), 529–546. <https://doi.org/10.1007/s00468-004-0339-6>
- Cescatti, A., Marcolla, B., Santhana Vannan, S. K., Pan, J. Y., Román, M. O., Yang, X., ... Schaaf, C. B. (2012). Intercomparison of MODIS albedo retrievals and in situ measurements across the global FLUXNET network. *Remote Sensing of Environment*, 121, 323–334. <https://doi.org/10.1016/j.rse.2012.02.019>
- Chu, H., Baldocchi, D. D., John, R., Wolf, S., & Reichstein, M. (2017). Fluxes all of the time? A primer on the temporal representativeness of FLUXNET: Fluxes all of the time? *Journal of Geophysical Research: Biogeosciences*, 122(2), 289–307. <https://doi.org/10.1002/2016JG003576>
- Coenders-Gerrits, A. M. J., van der Ent, R. J., Bogaard, T. A., Wang-Erlandsson, L., Hrachowitz, M., & Savenije, H. H. G. (2014). Uncertainties in transpiration estimates. *Nature*, 506(7487), E1–E2.
- Cowan, I. R., & Farquhar, G. D. (1977). Stomatal function in relation to leaf metabolism and environment. *Symposia of the Society for Experimental Biology*, 31, 471–505.
- De Kauwe, M. G., Medlyn, B. E., Pitman, A. J., Drake, J. E., Ukkola, A., Griebel, A., ... Roderick, M. (2019). Examining the evidence for decoupling between photosynthesis and transpiration during heat extremes. *Biogeosciences*, 16(4), 903–916. <https://doi.org/10.5194/bg-16-903-2019>
- Eller, C. B., Rowland, L., Oliveira, R. S., Bittencourt, P. R. L., Barros, F. V., da Costa, A. C. L., ... Cox, P. (2018). Modelling tropical forest responses to drought and El Niño with a stomatal optimization model based on xylem hydraulics. *Philosophical Transactions of the Royal Society B: Biological Sciences*, 373(1760), 20170315. <https://doi.org/10.1098/rstb.2017.0315>
- Fatichi, S., & Pappas, C. (2017). Constrained variability of modeled T:ET ratio across biomes: Transpiration:Evapotranspiration Ratio. *Geophysical Research Letters*, 44(13), 6795–6803.
- Fisher, J. B., Melton, F., Middleton, E., Hain, C., Anderson, M., Allen, R., ... Wood, E. F. (2017). The future of evapotranspiration: Global requirements for ecosystem functioning, carbon and climate feedbacks, agricultural management, and water resources: The future of evapotranspiration. *Water Resources Research*, 53(4), 2618–2626. <https://doi.org/10.1002/2016WR020175>
- Flo, V., Martinez-Vilalta, J., Steppe, K., Schuldt, B., & Poyatos, R. (2019). A synthesis of bias and uncertainty in sap flow methods. *Agricultural and Forest Meteorology*, 271, 362–374. <https://doi.org/10.1016/j.agrformet.2019.03.012>
- Friend, A. D., Arneeth, A., Kiang, N. Y., Lomas, M., Ogée, J., Rödenbeck, C., ... Zaehle, S. (2007). FLUXNET and modelling the global carbon cycle. *Global Change Biology*, 13(3), 610–633. <https://doi.org/10.1111/j.1365-2486.2006.01223.x>
- Good, S. P., Moore, G. W., & Miralles, D. G. (2017). A mesic maximum in biological water use demarcates biome sensitivity to aridity shifts. *Nature Ecology & Evolution*, 1(12), 1883–1888. <https://doi.org/10.1038/s41559-017-0371-8>
- Gorelick, N., Hancher, M., Dixon, M., Ilyushchenko, S., Thau, D., & Moore, R. (2017). Google Earth Engine: Planetary-scale geospatial analysis for everyone. *Remote Sensing of Environment*, 202, 18–27. <https://doi.org/10.1016/j.rse.2017.06.031>
- Hengl, T., Mendes de Jesus, J., Heuvelink, G. B. M., Ruiperez Gonzalez, M., Kilibarda, M., Blagotić, A., ... Kempen, B. (2017). SoilGrids250m: Global gridded soil information based on machine learning. *PLoS One*, 12(2), e0169748. <https://doi.org/10.1371/journal.pone.0169748>
- Huete, A., Didan, K., Miura, T., Rodriguez, E., Gao, X., & Ferreira, L. (2002). Overview of the radiometric and biophysical performance of the MODIS vegetation indices. *Remote Sensing of Environment*, 83(1–2), 195–213. [https://doi.org/10.1016/S0034-4257\(02\)00096-2](https://doi.org/10.1016/S0034-4257(02)00096-2)
- Jin, S., & Sader, S. A. (2005). Comparison of time series tasseled cap wetness and the normalized difference moisture index in detecting forest disturbances. *Remote Sensing of Environment*, 94(3), 364–372. <https://doi.org/10.1016/j.rse.2004.10.012>
- Jung, M., Reichstein, M., Margolis, H. A., Cescatti, A., Richardson, A. D., Arain, M. A., Arneeth, A., ... Williams, C. (2011). Global patterns of land-atmosphere fluxes of carbon dioxide, latent heat, and sensible heat derived from eddy covariance, satellite, and meteorological observations. *Journal of Geophysical Research*, 116. <https://doi.org/10.1029/2010JG001566>
- Jung, M., & Zscheischler, J. (2013). A guided hybrid genetic algorithm for feature selection with expensive cost functions. *Procedia Computer Science*, 18, 2337–2346. <https://doi.org/10.1016/j.procs.2013.05.405>
- Keenan, T. F., Hollinger, D. Y., Bohrer, G., Dragoni, D., Munger, J. W., Schmid, H. P., & Richardson, A. D. (2013). Increase in forest water-use efficiency as atmospheric carbon dioxide concentrations rise. *Nature*, 499(7458), 324–327.

- Knauer, J., Zaehle, S., Medlyn, B. E., Reichstein, M., Williams, C. A., Migliavacca, M., ... Linderson, M.-L. (2018). Towards physiologically meaningful water-use efficiency estimates from eddy covariance data. *Global Change Biology*, 24(2), 694–710. <https://doi.org/10.1111/gcb.13893>
- Kool, D., Agam, N., Lazarovitch, N., Heitman, J., Sauer, T., & Ben-Gal, A. (2014). A review of approaches for evapotranspiration partitioning. *Agricultural and Forest Meteorology*, 184, 56–70. <https://doi.org/10.1016/j.agrformet.2013.09.003>
- Kumar, J., Hoffman, F. M., Hargrove, W. W., & Collier, N. (2016). Understanding the representativeness of FLUXNET for upscaling carbon flux from eddy covariance measurements. *Earth System Science Data Discussions*, 1–25.
- Lasslop, G., Reichstein, M., Papale, D., Richardson, A. D., Arneeth, A., Barr, A., ... Wohlfahrt, G. (2010). Separation of net ecosystem exchange into assimilation and respiration using a light response curve approach: Critical issues and global evaluation: Separation of NEE into GPP and RECO. *Global Change Biology*, 16(1), 187–208. <https://doi.org/10.1111/j.1365-2486.2009.02041.x>
- Li, X., Gentine, P., Lin, C., Zhou, S., Sun, Z., Zheng, Y., ... Zheng, C. (2019). A simple and objective method to partition evapotranspiration into transpiration and evaporation at eddy-covariance sites. *Agricultural and Forest Meteorology*, 265, 171–182. <https://doi.org/10.1016/j.agrformet.2018.11.017>
- Lian, X., Piao, S., Huntingford, C., Li, Y., Zeng, Z., Wang, X., ... Wang, T. (2018). Partitioning global land evapotranspiration using CMIP5 models constrained by observations. *Nature Climate Change*, 8(7), 640–646. <https://doi.org/10.1038/s41558-018-0207-9>
- McCulloh, K. A., Winter, K., Meinzer, F. C., Garcia, M., Aranda, J., & Lachenbruch, B. (2007). A comparison of daily water use estimates derived from constant-heat sap-flow probe values and gravimetric measurements in pot-grown saplings. *Tree Physiology*, 27(9), 1355–1360. <https://doi.org/10.1093/treephys/27.9.1355>
- Medlyn, B. E., De Kauwe, M. G., Lin, Y.-S., Knauer, J., Duursma, R. A., Williams, C. A., ... Wingate, L. (2017). How do leaf and ecosystem measures of water-use efficiency compare? *New Phytologist*, 216(3), 758–770. <https://doi.org/10.1111/nph.14626>
- Medlyn, B. E., Duursma, R. A., Eamus, D., Ellsworth, D. S., Prentice, I. C., Barton, C. V. M., ... Wingate, L. (2011). Reconciling the optimal and empirical approaches to modelling stomatal conductance: Reconciling optimal and empirical stomatal models. *Global Change Biology*, 17(6), 2134–2144. <https://doi.org/10.1111/j.1365-2486.2010.02375.x>
- Meinshausen, N. (2006). Quantile regression forests. *Journal of Machine Learning Research*, 7(Jun), 983–999.
- Myneni, R., & Knyazikhin, Y. (2015). MCD15A3H MODIS/Terra+Aqua leaf area Index/FPAR 4-day L4 global 500m SIN grid V006.
- Nash, J., & Sutcliffe, J. (1970). River flow forecasting through conceptual models part I – A discussion of principles. *Journal of Hydrology*, 10(3), 282–290. [https://doi.org/10.1016/0022-1694\(70\)90255-6](https://doi.org/10.1016/0022-1694(70)90255-6)
- Nelson, J. A. (2019). Jnelson18/TranspirationEstimationAlgorithm: Force T to 0 at night. *Zenodo*. <https://doi.org/10.5281/ZENODO.2560321>
- Nelson, J. A. (2020a). Ecosystem transpiration from FLUXNET. *Zenodo*. <https://doi.org/10.5281/zenodo.3978408>
- Nelson, J. A. (2020b). Jnelson18/ecosystem-transpiration: Additional installation instructions. *Zenodo*. <https://doi.org/10.5281/ZENODO.3921923>
- Nelson, J. A., Carvalhais, N., Cuntz, M., Delpierre, N., Knauer, J., Ogée, J., & Jung, M. (2018). Coupling water and carbon fluxes to constrain estimates of transpiration: The TEA algorithm. *Journal of Geophysical Research. Biogeosciences*, 123, 3617–3632. <https://doi.org/10.1029/2018JG004727>
- Oren, R., Phillips, N., Katul, G., Ewers, B. E., & Pataki, D. E. (1998). Scaling xylem sap flux and soil water balance and calculating variance: A method for partitioning water flux in forests. *Annales des Sciences Forestières*, 55(1–2), 191–216. <https://doi.org/10.1051/forest:19980112>
- Paschalis, A., Fatichi, S., Pappas, C., & Or, D. (2018). Covariation of vegetation and climate constrains present and future T/ET variability. *Environmental Research Letters*, 13(10), 104012. <https://doi.org/10.1088/1748-9326/aae267>
- Pastorello, G., Papale, D., Chu, H., Trotta, C., Agarwal, D., Canfora, E., ... Torn, M. (2017). The FLUXNET2015 dataset: The longest record of global carbon, water, and energy fluxes is updated. *Eos*, 98.
- Paul-Limoges, E., Wolf, S., Schneider, F. D., Longo, M., Moorcroft, P., Gharun, M., & Damm, A. (2020). Partitioning evapotranspiration with concurrent eddy covariance measurements in a mixed forest. *Agricultural and Forest Meteorology*, 280, 107786. <https://doi.org/10.1016/j.agrformet.2019.107786>
- Perez-Priego, O., Katul, G., Reichstein, M., El-Madany, T. S., Ahrens, B., Carrara, A., ... Migliavacca, M. (2018). Partitioning eddy covariance water flux components using physiological and micrometeorological approaches. *Journal of Geophysical Research. Biogeosciences*, 123, 3353–3370. <https://doi.org/10.1029/2018JG004637>
- Pérez-Priego, O., Testi, L., Orgaz, F., & Villalobos, F. J. (2010). A large closed canopy chamber for measuring CO<sub>2</sub> and water vapour exchange of whole trees. *Environmental and Experimental Botany*, 68(2), 131–138. <https://doi.org/10.1016/j.envexpbot.2009.10.009>
- Perez-Priego, O., & Wutzler, T. (2019). ETpartitioning: Partitioning of eddy covariance ET into flux components. Retrieved from <https://github.com/oscarperezpriego/ETpartitioning>
- Pinty, B., Andreadakis, I., Clerici, M., Kaminski, T., Taberner, M., Verstraete, M. M., ... Widlowski, J.-L. (2011). Exploiting the MODIS albedos with the Two-stream Inversion Package (JRC-TIP): 1. Effective leaf area index, vegetation, and soil properties. *Journal of Geophysical Research*, 116(D9).
- Poyatos, R., Granda, V., Flo, V., Molowny-Horas, R., Steppe, K., Mencuccini, M., & Martínez-Vilalta, J. (2019). SAPFLUXNET: A global database of sap flow measurements. *Zenodo*. <https://doi.org/10.5281/zenodo.2530798>
- Poyatos, R., Granda, V., Molowny-Horas, R., Mencuccini, M., Steppe, K., & Martínez-Vilalta, J. (2016). SAPFLUXNET: Towards a global database of sap flow measurements. *Tree Physiology*, 36(12), 1449–1455. <https://doi.org/10.1093/treephys/tpw110>
- Reichstein, M., Falge, E., Baldocchi, D., Papale, D., Aubinet, M., Berbigier, P., ... Valentini, R. (2005). On the separation of net ecosystem exchange into assimilation and ecosystem respiration: Review and improved algorithm. *Global Change Biology*, 11(9), 1424–1439. <https://doi.org/10.1111/j.1365-2486.2005.001002.x>
- Scanlon, T. M., & Kustas, W. P. (2010). Partitioning carbon dioxide and water vapor fluxes using correlation analysis. *Agricultural and Forest Meteorology*, 150(1), 89–99. <https://doi.org/10.1016/j.agrformet.2009.09.005>
- Scanlon, T. M., Schmidt, D. F., & Skaggs, T. H. (2019). Correlation-based flux partitioning of water vapor and carbon dioxide fluxes: Method simplification and estimation of canopy water use efficiency. *Agricultural and Forest Meteorology*, 279, 107732. <https://doi.org/10.1016/j.agrformet.2019.107732>
- Schlesinger, W. H., & Jasechko, S. (2014). Transpiration in the global water cycle. *Agricultural and Forest Meteorology*, 189–190, 115–117. <https://doi.org/10.1016/j.agrformet.2014.01.011>
- Scott, R. L., & Biederman, J. A. (2017). Partitioning evapotranspiration using long-term carbon dioxide and water vapor fluxes: New approach to ET partitioning. *Geophysical Research Letters*, 44(13), 6833–6840. <https://doi.org/10.1002/2017GL074324>
- Sperry, J. S., Venturas, M. D., Anderegg, W. R. L., Mencuccini, M., Mackay, D. S., Wang, Y., & Love, D. M. (2017). Predicting stomatal responses to the environment from the optimization of photosynthetic gain and hydraulic cost: A stomatal optimization model. *Plant, Cell & Environment*, 40(6), 816–830. <https://doi.org/10.1111/pce.12852>

- Steppe, K., De Pauw, D. J., Doody, T. M., & Teskey, R. O. (2010). A comparison of sap flux density using thermal dissipation, heat pulse velocity and heat field deformation methods. *Agricultural and Forest Meteorology*, *150*(7–8), 1046–1056. <https://doi.org/10.1016/j.agrformet.2010.04.004>
- Stoy, P. C., El-Madany, T. S., Fisher, J. B., Gentine, P., Gerken, T., Good, S. P., ... Wolf, S. (2019). Reviews and syntheses: Turning the challenges of partitioning ecosystem evaporation and transpiration into opportunities. *Biogeosciences*, *16*(19), 3747–3775. <https://doi.org/10.5194/bg-16-3747-2019>
- Talsma, C. J., Good, S. P., Jimenez, C., Martens, B., Fisher, J. B., Miralles, D. G., ... Purdy, A. J. (2018). Partitioning of evapotranspiration in remote sensing-based models. *Agricultural and Forest Meteorology*, *260*–261, 131–143. <https://doi.org/10.1016/j.agrformet.2018.05.010>
- Tucker, C. J. (1979). Red and photographic infrared linear combinations for monitoring vegetation. *Remote Sensing of Environment*, *8*(2), 127–150. [https://doi.org/10.1016/0034-4257\(79\)90013-0](https://doi.org/10.1016/0034-4257(79)90013-0)
- Villalobos, F., Perez-Priego, O., Testi, L., Morales, A., & Orgaz, F. (2012). Effects of water supply on carbon and water exchange of olive trees. *European Journal of Agronomy*, *40*, 1–7. <https://doi.org/10.1016/j.eja.2012.02.004>
- Wang, L., Good, S. P., & Caylor, K. K. (2014). Global synthesis of vegetation control on evapotranspiration partitioning: Vegetation and ET partitioning. *Geophysical Research Letters*, *41*(19), 6753–6757. <https://doi.org/10.1002/2014GL061439>
- Wang, L., Good, S. P., Caylor, K. K., & Cernusak, L. A. (2012). Direct quantification of leaf transpiration isotopic composition. *Agricultural and Forest Meteorology*, *154*, 127–135. <https://doi.org/10.1016/j.agrformet.2011.10.018>
- Wei, Z., Yoshimura, K., Wang, L., Miralles, D. G., Jasechko, S., & Lee, X. (2017). Revisiting the contribution of transpiration to global terrestrial evapotranspiration: Revisiting global ET partitioning. *Geophysical Research Letters*, *44*(6), 2792–2801. <https://doi.org/10.1002/2016GL072235>
- Whelan, M. E., Lennartz, S. T., Gimeno, T. E., Wehr, R., Wohlfahrt, G., Wang, Y., ... Campbell, J. E. (2018). Reviews and syntheses: Carbonyl sulfide as a multi-scale tracer for carbon and water cycles. *Biogeosciences*, *15*(12), 3625–3657.
- Wilson, K. B., Hanson, P. J., Mulholland, P. J., Baldocchi, D. D., & Wullschlegel, S. D. (2001). A comparison of methods for determining forest evapotranspiration and its components: Sap-flow, soil water budget, eddy covariance and catchment water balance. *Agricultural and Forest Meteorology*, *106*(2), 153–168. [https://doi.org/10.1016/S0168-1923\(00\)00199-4](https://doi.org/10.1016/S0168-1923(00)00199-4)
- Zhou, S., Yu, B., Huang, Y., & Wang, G. (2014). The effect of vapor pressure deficit on water use efficiency at the subdaily time scale: Underlying water use efficiency. *Geophysical Research Letters*, *41*(14), 5005–5013. <https://doi.org/10.1002/2014GL060741>
- Zhou, S., Yu, B., Huang, Y., & Wang, G. (2015). Daily underlying water use efficiency for AmeriFlux sites: Daily underlying WUE. *Journal of Geophysical Research: Biogeosciences*, *120*(5), 887–902.
- Zhou, S., Yu, B., Zhang, Y., Huang, Y., & Wang, G. (2016). Partitioning evapotranspiration based on the concept of underlying water use efficiency: ET partitioning. *Water Resources Research*, *52*(2), 1160–1175. <https://doi.org/10.1002/2015WR017766>
- Zhou, S., Yu, B., Zhang, Y., Huang, Y., & Wang, G. (2018). Water use efficiency and evapotranspiration partitioning for three typical ecosystems in the Heihe River Basin, northwestern China. *Agricultural and Forest Meteorology*, *253*–254, 261–273. <https://doi.org/10.1016/j.agrformet.2018.02.002>
- Zhu, Z., Wang, S., & Woodcock, C. E. (2015). Improvement and expansion of the Fmask algorithm: Cloud, cloud shadow, and snow detection for Landsats 4–7, 8, and Sentinel 2 images. *Remote Sensing of Environment*, *159*, 269–277. <https://doi.org/10.1016/j.rse.2014.12.014>
- Zhu, Z., & Woodcock, C. E. (2012). Object-based cloud and cloud shadow detection in Landsat imagery. *Remote Sensing of Environment*, *118*, 83–94. <https://doi.org/10.1016/j.rse.2011.10.028>

## SUPPORTING INFORMATION

Additional supporting information may be found online in the Supporting Information section.

**How to cite this article:** Nelson JA, Pérez-Priego O, Zhou S, et al. Ecosystem transpiration and evaporation: Insights from three water flux partitioning methods across FLUXNET sites. *Glob Change Biol.* 2020;26:6916–6930. <https://doi.org/10.1111/gcb.15314>